



Earth-Adapter: Bridge the Geospatial Domain Gaps with Mixture of Frequency Adaptation

Xiaoxing Hu^{1*} Ziyang Gong^{2*} Yupei Wang^{1*†} Yuru Jia^{3,4} Gen Luo² Xue Yang^{5†}

¹Beijing Institute of Technology ²Shanghai AI Laboratory ³KU Leuven ⁴KTH ⁵Shanghai Jiao Tong University

*Equal Contribution †Corresponding Author

<https://github.com/VisionXLab/Earth-Adapter>

Abstract

Parameter-Efficient Fine-Tuning (PEFT) is a technique that allows us to adapt powerful Foundation Models (FMs) to diverse downstream tasks while preserving and unleashing their inherent capabilities. However, we have observed that existing PEFT methods, which are often designed with natural imagery in mind, struggle when applied to Remote Sensing (RS) scenarios. This is primarily due to their inability to handle artifact influences, a problem particularly severe in RS image features. To tackle this challenge, we introduce Earth-Adapter, the first PEFT method specifically designed for RS artifacts conquering. Earth-Adapter introduces a novel Mixture of Frequency Adaptation process that combines a Mixture of Adapter (MoA) with Discrete Fourier Transformation (DFT). By utilizing DFT, Earth-Adapter can decompose features into different frequency components, precisely separating artifacts from original features. The MoA then dynamically assigns weights to each adapter expert, allowing for the combination of features across various frequency domains. These simple-yet-effective approaches enable Earth-Adapter to more efficiently overcome the disturbances caused by artifacts than previous PEFT methods, significantly enhancing the FMs' performance on RS scenarios. Experiments on Domain Adaptation (DA), and Domain Generalization (DG) semantic segmentation benchmarks showcase the Earth-Adapter's effectiveness. Compared with baseline Rein, Earth-Adapter significantly improves 9.0% mIoU in DA and 3.1% mIoU in DG benchmarks. Our code will be released at [Earth-Adapter](#).

1. Introduction

Tremendous last year breakthroughs in Foundation Models (FMs) [3, 14, 22, 25, 38, 43, 51, 52] have ignited transformative progress in Computer Vision (CV), demonstrat-

ing unprecedented capabilities across both high-level and low-level vision tasks. Based on these FMs, considerable Remote Sensing (RS) research groups have also constructed large-scale, state-of-the-art (SOTA), and impressive Geospatial Foundation Models (GFMs) [5, 21, 23, 35, 41, 48, 62, 67], significantly promoting the development of RS imagery interpretation field. However, when adapting these FMs to downstream tasks, how to efficiently keep and unleash the power of FMs becomes a key problem. Under this context, Parameter-Efficient Fine-Tuning (PEFT) methods [8, 20, 28, 31, 36] become the pivotal method due to their superior parameter-performance trade-off.

Existing PEFT methods designed for language or nature imagery have made great progress with excellent works, such as LoRA [31], Visual Prompt Tuning (VPT) [36]. However, most of them show performance drops in RS cross-domain experiments. We argue the main reason lies in the influences of artifacts in the features. As shown in Figure 1 (a), we show the PCA visualization of features of DINOv2-L, which contains obvious redundant artifacts. Although a part of existing PEFT methods also are shown to be capable of handling artifacts [12], they still underestimate the artifact disturbances in RS imagery. The difference in the distribution of artifacts between natural and RS images is significant. In natural images, artifacts typically surround foreground objects [12], such as humans or animals, and the disturbances they cause are relatively limited. In contrast, RS images, due to their overhead perspective, lack centralized subjects and contain multiple coexisting multi-scale targets. For example, a single RS image may simultaneously include large-scale agricultural regions and fragmented road networks. As a result, artifacts are almost situated everywhere in RS images shown in Figure 1 (a), causing severe interference to domain-invariant representation learning, which is pivotal for cross-domain scenarios.

In our view, to address the influence of artifacts, one of the core ideas is to ‘divide-and-conquer’. Drawing on the

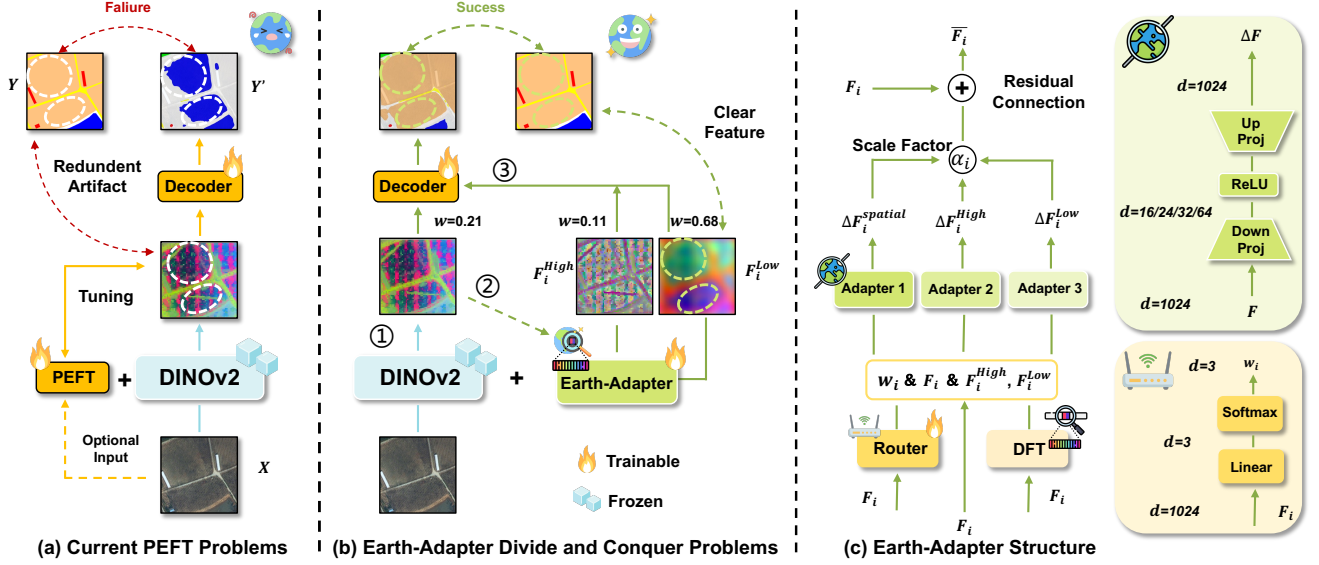


Figure 1. **Motivation and Structure Details of Earth-Adapter** (a) points out the artifact problems in existing PEFT methods. (b) illustrates how Earth-Adapter divides and conquers the artifacts by frequency-guided strategy and MoA framework. ①, ②, and ③ show the sequence of each step in the DFT operation. (c) introduces the details of the Earth-Adapter component structures.

principle that high-frequency (*HF*) signals encode local details (e.g., edge, contour) while low-frequency (*LF*) signals encode global structure (e.g., object surface), we leverage Discrete Fourier Transformation (DFT) as the ‘**divide**’ step. As illustrated in Figure 1 (b), we successfully leverage the DFT effectively to isolate artifacts into *HF* signals and splits coherent global features into *LF* signals. Subsequently, to ‘**Conquer**’ artifact-related issues, we adopt a Mixture of Adapter (MoA) architecture for PEFT design. The MoA router dynamically assigns weights to adapter experts, selecting the most relevant features for processing in each iteration. In this way, all features are aggregated into optimized representations, mitigating artifacts disturbances.

Based on our motivation and findings, we further present **Earth-Adapter**, a simple-yet-effective RS-specialized PEFT method designed for RS artifact conquering. Specifically, Earth-Adapter consists of a novel Mixture of Frequency Adapter architecture consisting of Mixture of Adapter (MoA) with Discrete Fourier Transformation (DFT). Earth-Adapter first disentangles geospatial features by DFT, and leverages multiple experts to conquer artifacts by adaptively aggregating and learning features with suitable frequency. In this fashion, Earth-Adapter can effectively alleviate the artifacts’ disturbances for robust domain-invariant feature learning. Then gradually introduces FMs to cross the geospatial gaps from the frequency perspective.

In experiments, we meticulously test Earth-Adapter on Domain Adaptation (DA), and Domain Generalization (DG) semantic segmentation tasks across five widely-used datasets. Comparing with existing PEFT methods, Earth-Adapter achieves State-Of-The-Art (SOTA) performance on

DA and DG benchmarks. In DA and DG benchmarks, Earth-Adapter outperforms our baseline Rein with 8.9% and 3.2% mIoU, respectively. Additionally, we also conduct in-depth analysis of the potential of Earth-Adapter. The core contributions can be summarized as follows:

- We propose a novel perspective to alleviate artifact-disturbance problems in RS imagery by frequency-guided divide-and-conquer strategy.
- We introduce a simple-yet-effective PEFT method, Earth-Adapter. It is also the first RS-specialized PEFT approach designed for cross-domain semantic segmentation tasks.
- Extensive comparisons validate the SOTA performance of Earth-Adapter on both DA and DG benchmarks. More ablation studies also demonstrate the high efficiency, robustness, and explainability of Earth-Adapter.

2. Related Work

2.1. RS Cross-Domain Semantic Segmentation

As a classical and fundamental task in the realm of computer vision, semantic segmentation [44, 54] not merely holds profound practical significance, but also provides an interface for researchers to dissect the high-level semantic representation of images. With the growing need for applying models to out-of-domain data, cross-domain segmentation, including domain adaptation (DA) [19, 29, 30, 39] and domain generalization (DG) [21, 64], has gained prominence. DA and DG are the two main paradigms, where DA aims to adapt a model from a labeled source domain to an unlabeled target domain, while DG focuses on training a model on only the source domain to generalize to unseen

target domains. In the RS field, cross-domain task is crucial due to the diversity of data, and lots of DA methods have been applied to improve the generalization ability of segmentation models, with applications in urban planning [53], land resource management [57], and environmental protection [55]. Compared with DA, the number of DG research [33, 40] in RS is much less than DA. Although these works [16, 34, 69] make contributions, most of them only focus on specialized models rather than leveraging the power of FMs, leading to limited cross-domain capabilities.

2.2. Geospatial Foundation Models

The emergence of Large Language Models (LLMs) [4] has prompted a shift in computer vision, leading to the development of Multimodal Large Language Models (MLLMs) [9, 42, 46, 51] and Vision Foundation Models (VFM) [24, 38, 43, 49]. FMs [3] in RS called GFMs [6, 26, 59–61] also can be divided into MLLMs and VFMs. Among MLLMs, RemoteCLIP [41] is the first exploration, supporting classification, retrieval, and object counting through a contrastive learning framework based on CLIP [51]. MetaEarth [67] advances diffusion models to generate multi-resolution RS images for any specified region based on both image and text conditions. Skysense [23] captures spatiotemporal information and performs well across diverse scenarios. Although these FMs obtain strong power by large-scale pertaining, how to effectively unleash their power to diverse downstream tasks is still a challenge.

2.3. PEFT in RS

PEFT approaches, such as adapter [27, 28, 31] are proposed to fine-tune large pre-trained models to downstream tasks in Natural Language Processing (NLP) by introducing lightweight learnable parameters. Subsequently, the PEFT has begun to be transferred to vision [1, 37, 66] tasks and rapidly become the focus of researchers. Visual Prompt Tuning (VPT) [36] first introduced ‘prompt tuning’ into the vision area as learnable vectors. The thought of this paradigm is also similar to the adversarial re-programming [15]. Currently, cross-domain works also focus on PEFT, such as [18] which is the first prompt tuning method in Domain Adaptation (DA) [17, 20, 56] and [64] is the first work leveraging PEFT to fine-tuning VFMs for Domain Generalization (DG) [2]. In the RS field, the exploration of PEFT is also vigorous. For example, UPetu [13] addresses storage for dense prediction tasks. TEA [32] uses an adapter network and top-down guidance for detection and segmentation tasks. [50] also leverage LoRA to solve oriented detection task. However, for the cross-domain semantic segmentation tasks, the research of PEFT is relatively blank, and existing methods can not handle the influence of artifacts. Earth-Adapter is the first PEFT for this area and can effectively tackle the artifacts.

3. Method

3.1. Preliminary

We first denote the input RS images as $\mathbf{x} \in \mathbb{R}^{H \times W \times 3}$, the corresponding label of \mathbf{x} as $\mathbf{y} \in \mathbb{R}^{H \times W \times K}$, and the semantic segmentation prediction of \mathbf{x} as $\mathbf{y}' \in \mathbb{R}^{H \times W \times K}$, where K represents the number of semantic classes. Here, we’ll illustrate our innovative Earth-Adapter overview.

The proposed Earth-Adapter is composed of two key components: the DFT and MoA. MoA consists of a *Spatial Adapter*, a *LF Adapter*, a *HF Adapter*, and a router. We employ R_ξ , parameterized by ξ , to denote the router and E_ϵ^i , $i \in \{1, 2, 3\}$, parameterized by ϵ , to represent the three adapter experts. For the network architecture, we adopt the framework introduced by Rein [64], integrating DINOv2 [49] as the backbone, represented as f_ϕ and parameterized by ϕ , alongside Mask2Former [10] as the decoder, denoted by f_θ and parameterized by θ . Section 3.2 illustrates the Earth-Adapter’s design, while Section 3.3 elaborates on our cross-domain training framework.

3.2. Details of Earth-Adapter

The core idea of Earth-Adapter is the seamless integration of highly efficient, learnable layers with minimal parameters into the frozen FMs.

Optimization objective. Before employing the Earth-Adapter, the optimization objective of fine-tuning FMs is to identify a set of parameters that minimize the loss of the entire model on the downstream task:

$$\arg \min_{\theta} \sum_{(\mathbf{x}, \mathbf{y}) \in \mathcal{D}} \mathcal{L}_{\text{seg}}(f_\theta(f_\phi(\mathbf{x})), \mathbf{y}), \quad (1)$$

where \mathcal{D} is the dataset, $f_\phi \cdot f_\theta$ is the segmentation model, and \mathcal{L}_{seg} is the loss function, here we use the default CE loss. After activating our Earth-Adapter, the optimization objective becomes:

$$\arg \min_{\theta, \epsilon, \xi} \sum_{(\mathbf{x}, \mathbf{y}) \in \mathcal{D}} \mathcal{L}_{\text{seg}} \left(f_\theta \left(\underbrace{R_\xi \circ E_\epsilon}_{\text{Earth-Adapter}}(f_\phi^*(\mathbf{x})) \right), \mathbf{y} \right). \quad (2)$$

During training, the original parameters of the backbone are kept frozen (denoted as f_ϕ^*), ensuring they remain unaltered. In the following description, we denote the segmentation network combined with Earth-Adapter as $G_{\theta, \xi, \epsilon}$.

Parallel Frequency Adaptation. Let $\mathbf{F}_i \in \mathbb{R}^{n \times c}$ denote the visual feature at the i -th layer of the backbone, where n represents the token sequence length and c denotes the channel dimension. Our frequency adaptation operates through parallel processing streams: The first *Spatial Adapter* employs a low-rank projection to refine the spatial feature:

$$\Delta \mathbf{F}_i^{\text{spatial}} = \text{Adapter}_1^i(\mathbf{F}_i^T), \quad (3)$$

where $\Delta \mathbf{F}_i^{spatial}$ means the processed i -th layer Spatial-Domain features, and **Adapter**₁ represents a nonlinear mapping layer composed of two low-rank matrices:

$$\mathbf{Adapter}_i = \mathbf{W}_{up}(\text{Relu}(\mathbf{W}_{down}(\cdot))). \quad (4)$$

The *Frequency Adapter* decompose features through spectral analysis. We first reshape $\mathbf{F}^{spatial}$ to (C, H, W) and apply DFT on spatial features as $\mathcal{FT}(\mathbf{F}^{spatial})$. When splitting the frequency domains, we employ a fixed frequency cutoff ρ to decompose the spectrum into high and low frequency components. Subsequently, these components are transformed back into features via the Inverse Fourier Transform (IFT), yielding *LF* and *HF* features:

$$\mathbf{F}_i^{low} = \mathcal{FT}^{-1}(\mathbf{M} \odot \mathcal{FT}(\mathbf{F}^{spatial})), \quad (5)$$

$$\mathbf{F}_i^{high} = \mathcal{FT}^{-1}((1 - \mathbf{M}) \odot \mathcal{FT}(\mathbf{F}^{spatial})). \quad (6)$$

The frequency mask $\mathbf{M} \in \{0, 1\}^{H \times W}$ is defined by:

$$\mathbf{M}(u, v) = \begin{cases} 1 & , \text{ if } \max(|u - \frac{H}{2}|, |v - \frac{W}{2}|) \leq \rho \frac{H}{2} \\ 0 & , \text{ otherwise} \end{cases} \quad (7)$$

Thereafter, the *LF* and *HF* features are independently passed through two distinct low-rank linear projection layers, generating frequency adaptation adjustments:

$$\Delta \mathbf{F}_i^{low} = \text{Adapter}_2^i(\mathbf{F}_i^{low}), \quad (8)$$

$$\Delta \mathbf{F}_i^{high} = \text{Adapter}_3^i(\mathbf{F}_i^{high}). \quad (9)$$

Mixture of Adapters. We implement dynamic feature fusion through a Router that learns optimal combinations of feature adjustment according to the original visual features. The Router weight is computed by channel-wise attention:

$$\mathbf{w}_i = \text{Softmax}(R_\xi(\mathbf{F}_i)), \quad (10)$$

where \mathbf{w}_i represents weights for *spatial*, *LF*, and *HF* components. The final feature adjustment is calculated as:

$$\Delta \mathbf{F}_i = \alpha_i \sum_{k=1}^3 \mathbf{w}^{(k)} \Delta \mathbf{F}_i^{(k)}, \quad (11)$$

where α_i is a learnable scaling parameter with small initial value, and $k \in \{spatial, low, high\}$. The complete feature optimization also maintains residual structure:

$$\bar{\mathbf{F}}_i = \mathbf{F}_i + \Delta \mathbf{F}_i. \quad (12)$$

3.3. Training Framework

In this study, we explore the application of Earth-Adapter across two distinct tasks: DG and UDA Semantic Segmentation. For Supervised and DG Semantic Segmentation

tasks, we train Earth-Adapter with Mask2former in end-to-end supervised learning as Equation 2. For UDA Semantic Segmentation, we use the self-training framework introduced in DACS [58] without using target domain labels. The pseudo labels for target domain images are produced by a teacher network $G_{\theta, \xi, \epsilon}^\dagger$:

$$\bar{\mathbf{y}}_{\mathbf{T}}^{(j, k)} = [k = \arg \max_{k'} G_{\theta, \xi, \epsilon}^\dagger(\mathbf{x}_{\mathbf{T}})]^{(j, k')}, \quad (13)$$

where $[\cdot]$ denotes the Iverson bracket, and $j \in HW$ is the spatial index of the pixel in the image. The teacher network remains inactive during the training process, with its parameters being updated based on an exponential moving average (EMA) of the student model's parameters:

$$G_{\theta, \xi, \epsilon, t+1}^\dagger = \alpha G_{\theta, \xi, \epsilon, t}^\dagger + (1 - \alpha) G_{\theta, \xi, \epsilon, t} \quad (14)$$

Here t denotes the t_{th} training iteration. The hyperparameter α controls the update speed of the teacher network's parameters. After obtaining the pseudo-labels, we perform category-wise mixing of samples from the source and target domains:

$$\begin{aligned} \mathbf{x}_{mix} &= \mathbf{x}_{\mathbf{S}} \odot \mathcal{M} + \mathbf{x}_{\mathbf{T}} \odot (1 - \mathcal{M}) \\ \mathbf{y}_{mix} &= \mathbf{y}_{\mathbf{S}} \odot \mathcal{M} + \bar{\mathbf{y}}_{\mathbf{T}} \odot (1 - \mathcal{M}) \end{aligned} \quad (15)$$

where $(\mathbf{x}_{\mathbf{S}}, \mathbf{y}_{\mathbf{S}})$ is the data sample from the source domain, and \mathcal{M} is generated by randomly selecting half of the categories based on the labels of the source domain $\mathbf{y}_{\mathbf{S}}$. The Optimization objective for the UDA task is defined by:

$$\begin{aligned} \arg \min_{\theta, \xi, \epsilon} \sum_{(\mathbf{x}, \mathbf{y}) \in \mathcal{D} \cup \mathcal{D}_{mix}} \mathcal{L}_{\text{seg}}(G_{\theta, \xi, \epsilon}(\mathbf{x}), \mathbf{y}) \\ + \lambda_{uda} \mathcal{L}_{\text{seg}}(G_{\theta, \xi, \epsilon}(\mathbf{x}_{mix}), \mathbf{y}_{mix}). \end{aligned} \quad (16)$$

λ_{uda} is the weight parameter for UDA loss.

4. Experiments

4.1. Experimental setup

Datasets and Benchmark. We conduct all experiments on several widely used remote sensing image segmentation datasets: Potsdam [47] and Vaihingen [47], both created by the International Society for Photogrammetry and Remote Sensing (ISPRS) and LoveDA [63]. The Potsdam dataset includes 38 very high resolution (VHR) True Orthophotos (TOP) images with $6,000 \times 6,000$ pixels. The Potsdam dataset has different imaging modes including IR-R-G channels, R-G-B channels, and R-G-B-IR channels. We use the RGB band for the following experiments. The Vaihingen dataset consists of 33 VHR TOP images with an average size of $2,494 \times 2,064$ pixels. The LoveDA dataset comprises a total of 4,190 images, each with a resolution of $1,024 \times 1,024$ pixels. Based on the aforementioned dataset,

| Backbone | Methods | Cross-Domain Adaptation | | | | Avg. | Cross-Domain Generalization | | | | Avg. |
|-----------------------------------|----------------------|-------------------------|--------------------|--------------------|---------------------|--------------------|-----------------------------|--------------------|--------------------|--------------------|--------------------|
| | | P2V | V2P | R2U | U2R | | P2V | V2P | R2U | U2R | |
| MiT-B5 [65] | DAFormer [29] | 64.4 | 54.8 | 52.7 | 42.5 | 53.6 | 42.4 | 41.4 | 54.2 | 39.9 | 44.5 |
| | HRDA [30] | 67.6 | 58.6 | 53.2 | 35.3 | 53.7 | 33.1 | 31.1 | 54.2 | 39.8 | 39.6 |
| DINOv2-L [49] | Frozen | 21.0 | 7.2 | 21.5 | 11.8 | 15.4 | 57.9 | 49.4 | 57.1 | 42.7 | 51.8 |
| | Full Fine-Tune | 11.3 | 16.5 | 23.1 | 10.6 | 15.4 | 12.6 | 19.6 | 33.1 | 19.7 | 21.3 |
| | Adapter [28] | 66.4 | 59.3 | 55.9 | 46.2 | 57.0 | 56.0 | 47.4 | 57.6 | 41.8 | 50.7 |
| | LoRA [31] | 17.8 | 18.8 | 24.5 | 26.0 | 15.7 | 20.3 | 25.6 | 29.3 | 21.9 | 24.3 |
| | VPT [36] | 66.2 | 59.3 | 55.3 | 48.0 | 57.2 | 59.2 | 52.3 | 57.4 | 44.9 | 53.5 |
| | AdaptFormer [7] | 12.9 | 15.3 | 25.1 | 22.2 | 18.9 | 14.0 | 19.3 | 31.0 | 15.8 | 20.0 |
| | Rein (Baseline) [64] | 60.2 | 60.9 | 52.8 | 26.0 | 50.0 | 60.8 | 52.5 | 55.8 | 43.4 | 53.1 |
| | Earth-Adapter (Ours) | 67.7 (+7.5) | 62.2 (+1.3) | 55.9 (+3.1) | 50.0 (+24.0) | 59.0 (+9.0) | 64.9 (+4.1) | 55.1 (+2.6) | 59.0 (+3.2) | 45.7 (+2.3) | 56.2 (+3.1) |
| Improvements over the second best | | +0.1 | +1.3 | +0.0 | +2.0 | +1.8 | +4.1 | +2.5 | +1.4 | +0.8 | +2.7 |

Table 1. **Performance Comparison between representative DA models, PEFT methods, and our Earth-Adapter on DA and DG benchmarks.** The **Bold** font in the table means the SOTA performance. The ‘+’ in the bracket means the improvement compared with our baseline Rein. The last line of data means the improvement compared with the second-best performance of all other methods.

| Methods | Setting | Surf | Bldg | Vegt | Tree | Car | Clut | mIoU (%) | Setting | Bkgd | Bldg | Road | Water | Barr | Frst | Agri | mIoU (%) |
|----------------------|-------------|-------------|-------------|-------------|-------------|-------------|-------------|-------------|---------|-------------|-------------|-------------|-------------|-------------|-------------|-------------|-------------|
| Frozen | P2V (DA) | 38.6 | 24.1 | 11.9 | 47.2 | 2.5 | 1.5 | 21.0 | U2R | 42.6 | 17.2 | 6.7 | 9.6 | 0.7 | 5.7 | 0.0 | 11.8 |
| Rein [64] | | 75.4 | 88.6 | 50.3 | 73.4 | 59.0 | 14.5 | 60.2 | (DA) | 27.9 | 41.9 | 29.3 | 51.2 | 0.8 | 53.2 | 0.0 | 29.2 |
| Earth-Adapter (Ours) | | 80.3 | 89.5 | 66.3 | 74.4 | 61.9 | 33.6 | 67.7 | | 56.3 | 63.4 | 48.7 | 66.6 | 13.7 | 38.4 | 63.2 | 50.0 |
| Frozen | P2V (DG) | 70.6 | 79.9 | 46.1 | 72.1 | 58.6 | 20.4 | 57.9 | U2R | 56.7 | 54.8 | 41.3 | 67.0 | 14.6 | 15.1 | 49.2 | 42.7 |
| Rein [64] | | 74.4 | 85.1 | 51.0 | 23.0 | 57.1 | 24.5 | 60.8 | (DG) | 53.0 | 57.8 | 41.2 | 61.1 | 9.4 | 23.4 | 57.8 | 43.4 |
| Earth-Adapter (Ours) | | 76.3 | 85.4 | 59.0 | 74.1 | 54.2 | 40.6 | 64.9 | | 52.6 | 55.7 | 44.1 | 64.6 | 17.0 | 29.6 | 56.1 | 46.7 |

Table 2. **Performance Comparison of Per-Class between Frozen DINOv2-L, Rein, and Earth-Adapter on Potsdam RGB-to-Vaihingen.** Both Rein and ours are based on the Frozen DINOv2-L. The **Bold** font means the best performance.

| Backbone | Methods | Params | P2V(DG) | V2P(DG) | Avg. |
|--------------------------|----------------|--------|-------------|-------------|--------------------|
| CLIP [51] (ViT-Large) | Frozen | 0.0M | 43.7 | 44.4 | 44.1 |
| | Full Fine-Tune | 304.2M | 11.4 | 20.3 | 15.9 |
| | Earth-Adapter | 2.4M | 49.7 | 50.2 | 50.0 (+5.9) |
| DINOv2 [49] (Small) | Frozen | 0.0M | 44.3 | 43.3 | 43.8 |
| | Full Fine-Tune | 22.1M | 41.9 | 41.8 | 41.9 |
| | Earth-Adapter | 2.4M | 47.5 | 44.8 | 46.2 (+2.4) |
| DINOv2 [49] (Base) | Frozen | 0.0M | 51.4 | 49.5 | 50.5 |
| | Full Fine-Tune | 86.6M | 46.7 | 49.8 | 49.8 |
| | Earth-Adapter | 2.4M | 53.0 | 51.8 | 52.4 (+1.9) |
| DINOv2 [49] (Large) | Frozen | 0.0M | 57.9 | 49.4 | 53.7 |
| | Full Fine-Tune | 304.2M | 12.6 | 19.6 | 16.1 |
| | Earth-Adapter | 2.4M | 64.9 | 55.1 | 60.0 (+6.3) |

Table 3. **Ablation studies of Earth-Adapter on different foundation backbones.** Both P2V and V2P are the DG benchmarks. Results validate that Earth-Adapter’s effectiveness on diverse backbone networks.

we follow MMSegmentation settings to split the train and val sets, crop images, and establish four benchmarks including both DA and DG: **Potsdam to Vaihingen** (P2V), **Vaihingen to Potsdam** (V2P), **Rural to Urban** (R2U), **Urban to Rural** (U2R). In our experimental setup, all images are cropped to a size of 512×512 .

Implementation Details. We use MMSegmentation [11] as our training and evaluation framework. We employ Mask2former [10] as our decoder, which is a highly efficient and effective algorithm for semantic segmentation tasks. For backbone, we utilize the Dinov2 [49] series models to extract features, which are subsequently utilized

| Adapter | + HF | + LF | P2V (DG) | V2P (DG) | Avg. |
|---------|------|------|-------------|-------------|--------------------|
| 1 | - | - | 61.0 | 52.8 | 56.9 (+0.0) |
| - | 1 | - | 59.4 | 50.9 | 50.9 (-6.0) |
| - | - | 1 | 59.1 | 51.5 | 55.3 (-1.6) |
| 2 | - | - | 61.6 | 51.4 | 56.5 (-0.4) |
| 3 | - | - | 64.0 | 52.7 | 58.4 (+1.5) |
| 4 | - | - | 61.4 | 53.3 | 57.4 (+0.5) |
| 5 | - | - | 62.5 | 52.5 | 57.5 (+0.6) |
| 1 | 1 | 1 | 64.9 | 55.1 | 60.0 (+3.1) |
| 2 | 1 | 1 | 61.3 | 54.7 | 58.0 (+1.1) |
| 3 | 1 | 1 | 61.6 | 54.6 | 58.1 (+1.2) |

Table 4. **Ablation of Adapters’ Combination.** The ‘Adapter’ means the number of vanilla Adapter that accepts *Spatial* features. The ‘+ HF’ and ‘+ LF’ represent the number of adapters that accept high and low-frequency features as input. The ‘+’ in the bracket represents the gain compared with one **Adapter**.

as input for the Mask2former. During training, we utilize AdamW [45] as the optimizer, with a learning rate of $1e-5$ for the backbone, $1e-4$ for the decoder, and $1e-4$ for the relevant parameters in PEFT. Within the DACS training framework, we set α to 0.99 and λ_{uda} to 0.5.

4.2. Cross-Domain Performance Comparison

As depicted in Table 1, we conduct a comparative analysis of the existing mainstream PEFT methods, such as Adapter [28], LoRA [31], and VPT [36], against our Earth-Adapter across eight cross-domain benchmarks, with state-of-the-art method Rein [64] in natural scene as our base-

| Backbone | Methods | Params ↓ | Train Speed (s/iter) ↓ | Infer Speed (s/iter) ↓ | mIoU (%) ↑ |
|----------|---------------|-----------------|------------------------|------------------------|--------------------|
| DINOv2-L | Full | 304.2M | 0.80 | 0.11 | 15.4 |
| | Rein | 3.0M | 0.68 | 0.12 | 50.0 |
| | Earth-Adapter | 2.3M(1.0M~3.9M) | 0.71 | 0.12 | 59.0 (+9.0) |

Table 5. **Comparison on Parameters, Speed, and Performance between FFT, Rein, and Earth-Adapter.** All results are the average score of DA benchmarks, demonstrating the excellent trade-off of Earth-Adapter.

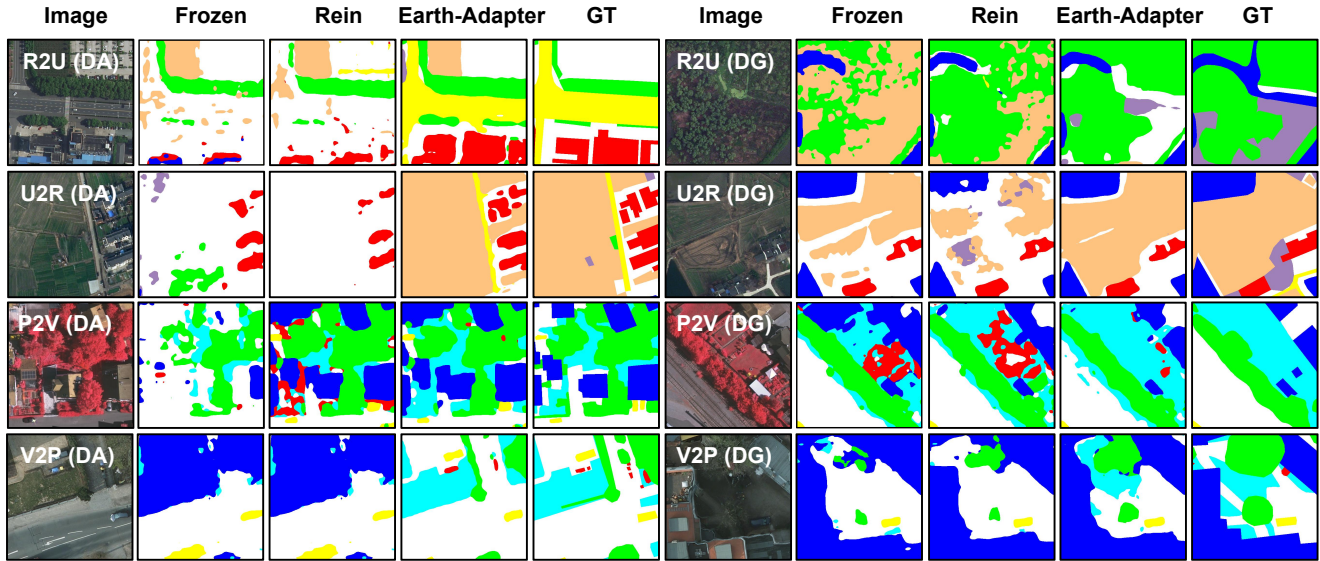


Figure 2. **Visualization of Predicted Segmentation Maps** We Compare Earth-Adapter with the Frozen DINOv2-L backbone and our baseline Rein on eight cross-domain benchmarks. For the Potsdam and Vaihingen color map, white is the Impervious surface, red is the clutter, blue is the building, cyan is the low vegetation, green is the tree, and yellow is the car. For LoveDA color map, red is the building, yellow is the road, blue is the water, purple is the barren, green is the forest, brown is the agriculture.

line. These benchmarks encompass four DA scenarios (P2V, V2P, R2U, and U2R) and four DG scenarios that mirror the DA ones.

Starting with the DA experiments, when compared to the performance of DA-specialized models, a significant number of existing PEFT methods exhibit performance collapse. For instance, LoRA achieves only 17.8% mIoU in the P2V (DA) benchmark when handling RS (Remote Sensing) images, a figure even lower than that of the Frozen backbone DINOv2-L. A similar trend is observed in Full Fine-Tuning, AdaptFormer, and Rein. We posit that this issue may stem from the DA self-training paradigm, which involves intensive image-mixing operations that these PEFT methods struggle to adapt to. However, two PEFT methods, Adapter and Rein, demonstrate relatively robust performance in the DA setting. When compared to these methods, our Earth-Adapter proves to be more effective in adapting to target domains. It outperforms baseline Rein by 7.5% mIoU in P2V, 3.1% mIoU in R2U, 24.0% mIoU in U2R, and 9.0% mIoU on average across the DA benchmarks. Notably, in the U2R (DA) benchmark, Earth-Adapter significantly mitigates the collapse of Rein, boosting the mIoU from 26.0%

to 50.0%.

Shifting to the DG experiments, the performance collapse persists, though the trend is somewhat alleviated. In contrast to DA, the Frozen model reveals the potential generalizability of DINOv2-L. Nevertheless, FFT, LoRA, and AdaptFormer still exhibit limitations. On the other hand VPT, and Rein continue to show strong transfer capabilities, achieving 53.5% and 53.1% mIoU on average, surpassing the Frozen model by 1.7%, and 1.3% mIoU. Similar to the DA benchmark, Earth-Adapter also achieves state-of-the-art (SOTA) performance in DG, with improvements of 3.1% and 4.4% mIoU over the baseline Rein and Adapter, respectively.

4.3. Ablation Study

Analysis on Per-class Performance. In this part, we demonstrate the detailed performance of each class on four benchmarks: P2V (DA), P2V (DG), U2R (DA), and U2R (DG) between Frozen DINOv2-L, Rein, and our Earth-Adapter. All the results are shown in Table 2, and we first discuss the P2V experiment results.

In the P2V (DA), both Rein and Earth-Adapter show

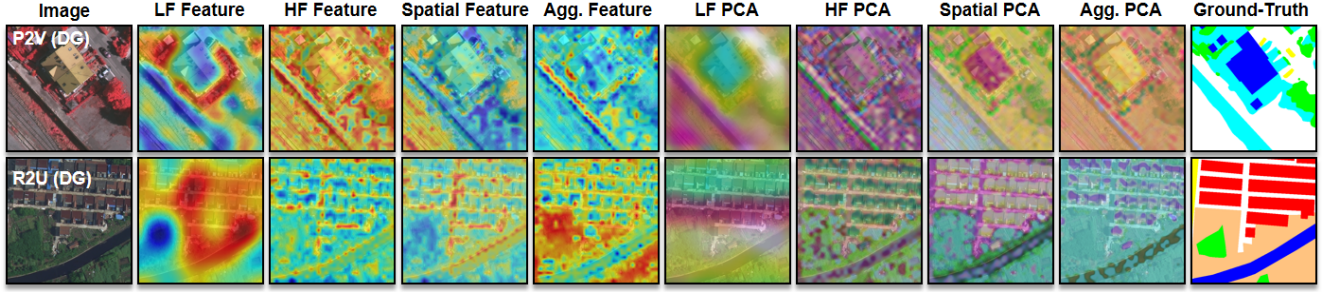


Figure 3. **Visualization and PCA of Adapters' Feature Maps.** 'Agg. Feature' represents the aggregated adapters' features. 'PCA' represents the Principal Component Analysis of features. All visualizations represent feature maps, not heatmaps. Thus only the semantic boundaries within the features should be focused rather than color intensities.

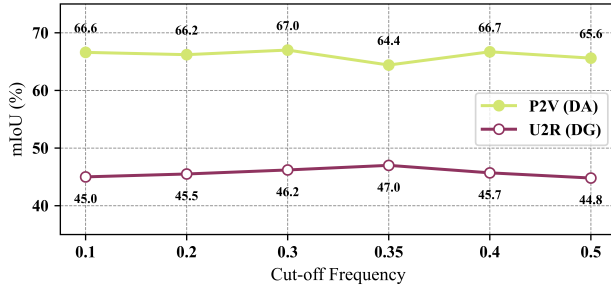


Figure 4. **Parameter-sensitive experiments of the cut-off frequency of DFT.** The results on P2V (DA) and U2R (DG) benchmarks show Earth-Adapter's robustness to the cut-off frequency.

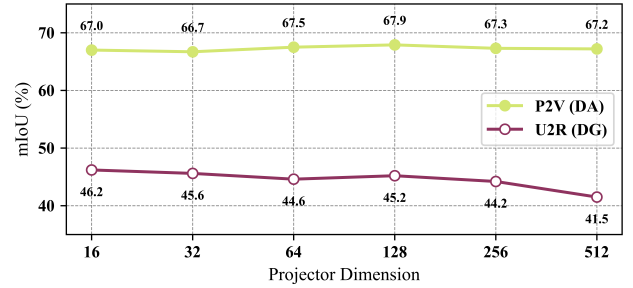


Figure 5. **Parameter-sensitive experiments of the projector dimension in Adapter.** The results on P2V (DA) and U2R (DG) benchmarks show Earth-Adapter's robustness to dimensions.

significant improvement on the Vegetation class compared with the Frozen DINOv2-L. Nevertheless, Earth-Adapter achieves a much higher performance than Rein, with 7.5% mIoU. A similar trend can be observed in the P2V (DG), where Earth-Adapter surpasses the other two methods by 7.0% and 4.1% mIoU respectively. Looking at the performance changes of the Vegetation and Tree classes, something interesting stands out. In the P2V (DA), both Earth-Adapter and Rein perform better on the Tree class than the Frozen. In contrast, in the P2V (DG), the performance of the Frozen with Rein on the Tree class drops drastically from 74.1% to 23.0% mIoU. As indicated in prior research [21], Rein's features struggle to distinguish between the Vegetation and Tree classes due to their similar appearance from the RS perspective, especially in DG setting which faces more unpredictable domain shifts than DA. Moreover, in P2V (DG), comparing Rein with the Frozen, almost all other classes improve except for the Tree class. Thus, it can be empirically inferred that the improvement of the Vegetation class by Rein comes at the cost of a decline in the performance of the Tree class. However, Earth-Adapter can reduce this negative impact. It does this by optimizing the representation to tell the two classes apart and boost their performance.

In the LoveDA experiments, as previously discussed, both the Frozen and Rein methods suffer from performance collapse in the U2R (DA) setting. When examining the performance at a more class level, it becomes evident that the primary decline for Rein occurs in the Barren and Agriculture classes. The performance drop in the Barren class can be attributed to it being the most sparse class within the LoveDA dataset. However, the performance of both the Frozen and Rein methods on the Agriculture class is a concerning 0.0% mIoU. In our opinion, the main factor probably is the presence of artifacts, as illustrated in Figure 1. Most PEFT methods from the CV field are unable to effectively handle the disturbances caused by these artifacts. Nevertheless, Earth-Adapter is capable of effectively utilizing the target domain data, achieving a notable 13.7% mIoU in the Barren class. Furthermore, as depicted in Figure 1, Earth-Adapter has a significant advantage with its frequency-domain divide-and-conquering ability, which enables it to improve the Agriculture performance from 0 to 63.2% mIoU. In the U2R (DG) experiments, both the Frozen and Rein methods demonstrate their effectiveness and significantly address the issues present in the DA setting. Additionally, Earth-Adapter achieves SOTA performance with improvements across most classes.

| Benchmark | Adapter dim | Cutoff frequency | Activation layer | mIoU(%) |
|-----------|-------------|------------------|--------------------------|---------|
| P2V (DA) | 64 | 0.3 | [0, 1, 2] | 67.7 |
| P2V (DG) | 24 | 0.3 | [18, 19, 20, 21, 22, 23] | 64.9 |
| V2P (DA) | 32 | 0.2 | [21, 22, 23] | 62.2 |
| V2P (DG) | 64 | 0.3 | [18, 19, 20, 21, 22, 23] | 55.1 |
| R2U (DA) | 16 | 0.3 | [21, 22, 23] | 55.9 |
| R2U (DG) | 64 | 0.3 | [18, 19, 20, 21, 22, 23] | 59.0 |
| U2R (DA) | 32 | 0.2 | [18, 19, 20, 21, 22, 23] | 50.0 |
| U2R (DG) | 64 | 0.3 | [21, 22, 23] | 45.7 |

Table 6. Hyperparameter Configuration of dimension, cutoff frequency, and activation layer of Frequency Adapters in Earth-Adapter. Notably, Spatial Adapter is activated in all backbone layers. All the results are the best performance.

Performance on Different Backbones. Besides the DINOv2-L backbone in Table 1, Earth-Adapter is also applied to CLIP (ViT-L) and other DINOv2 scales: ViT-Small and ViT-Base, with results in Table 3. These results show Earth-Adapter improves performance across diverse backbones with varying parameter scales. Notably, Earth-Adapter achieves larger improvements on larger models, such as ViT-L, with 7.0% and 5.7% mIoU gains, more than those on small and base scale ViTs. This suggests Earth-Adapter has a greater performance upper bound.

Prediction Visualization Analysis. In Figure 2, we visualize the predicted segmentation map of the Frozen DINOv2-L, Rein, and Earth-Adapter. It is worth noting that in the U2R (DG) example, Rein’s prediction is worse than the original backbone, which means Rein can not adapt to RS image well, which leads to a negative effect on the backbone features. In contrast, on the backbone’s basement, the Earth-Adapter keeps the good details of backbone features, and further optimizes the representation of agriculture class. And in other experiments, Earth-Adapter also exhibits better prediction than Rein and Frozen backbone, showing a higher performance upperbound.

Feature Visualization Analysis. In Figure 3, we visualize features captured by three adapters on P2V (DG) and R2U (DG) benchmarks. As discussed in the introduction, *LF* features focus on coarse-grained and global semantics, while *HF* features show detailed representations. The aggregated features are a weighted summation of the three different frequency features. PCA visualizations clearly show each feature’s characteristics. Take P2V in the figure as an example, artifacts are almost filtered into high-frequency features (shown in ‘*HF* PCA’), and dynamic fusion of all features ensures the final aggregated features’ PCA maintains clear semantic edges and successfully filters out artifacts. These visualizations further enhance Earth-Adapters’ explainability.

Component Effectiveness Ablation. In Table 4, ablation studies on MoA’s components and adapter numbers show that using only *HF* or *LF* adapters decreases performance compared to spatial adapters, with *HF* causing a larger drop. This aligns with PCA visualizations in

| Layer | Adapter | | Earth-Adapter | |
|--------------------------|----------|----------|---------------|----------|
| | U2R (DA) | R2U (DG) | U2R (DA) | R2U (DG) |
| Frozen | 11.8 | 57.1 | 11.8 | 57.1 |
| [0, 1, 2, 3, 4, 5] | 44.7 | 57.4 | 47.6 | 59.0 |
| [18, 19, 20, 21, 22, 23] | 46.0 | 58.1 | 50.0 | 58.5 |

Table 7. Layer effect comparison between Adapter and Earth-Adapter. The results show Earth-Adapter learns better under the same layer setting.

1 (b) and 3, where *HF* features have more artifacts and noise, while *LF* features are smooth with clear global semantics. Thus, using only *HF* severely damages performance. Although only using *LF* features outperforms *HF* features (50.9% mIoU), it still underperforms *spatial* features (56.9% mIoU) due to lacking semantic details. After that, we also conduct more experiments on the number of *Spatial* adapters, and reveal the best composition is the one *spatial* adapter with one *HF* and *LH* adapters.

Performance-Speed Trade-Off Ablation. We compare the parameters, speed, and performance between FFT, Rein, and Earth-Adapter in Table 5. Significantly, at the same time of close training and inference speed with Rein, Earth-Adapter achieves better performance (9.0% mIoU improvement), with a smaller parameter scale.

Hyper-Parameter Sensitive Ablation. In this section, we conduct an ablation study to test Earth-Adapter with two hyper-parameter variations on both the P2V (DA) and U2R (DG) benchmarks. Figure 4 presents the studies of the cut-off frequency with the dimension as 16, and Figure 5 illustrates the studies of the projector dimension in the Adapter with the cut-off frequency as 0.3. Both experiments show a consistent trend: Earth-Adapter shows greater robustness in the DA than in the DG setting. We posit that this occurs because the DA task inherently possesses higher certainty compared to DG. In the DA, even when hyper-parameters are altered, Earth-Adapter can effectively learn from the augmented target domain data, thereby maintaining performance stability. Despite DG’s uncertainty, Earth-Adapter shows a relatively stable performance in a certain parameter range. For instance, when the cut-off frequency is between 0.3 and 0.4, performance fluctuations are minimal. Similarly, for the projector dimension, performance is stable across a broad range from 16 to 256 and only fluctuates when the dimension is 512. Importantly, there are no other hyper-parameters requiring tuning. These results underscore Earth-Adapter’s superiority in handling parameter variations, offering a reliable solution for both DA and DG.

4.4. Analysis of Overall Parameter Configuration.

The detailed hyperparameter configurations for each benchmark are presented in Table 6. Overall, our method demonstrates exceptional robustness, exhibiting relatively low sensitivity to parameter variations. Below we provide an in-

| Spatial Adapter | MoA | Frequency Layer | Cutoff Frequency | U2R (DA) | V2P (DA) | P2V (DG) | R2U (DG) |
|-----------------|-----|-----------------|------------------|-------------|-------------|-------------|-------------|
| ✓ | - | - | - | 48.6 | 60.1 | 61.0 | 58.6 |
| ✓ | ✓ | Full | 0.3 | 47.0 | <u>60.9</u> | 61.3 | 58.1 |
| ✓ | ✓ | shallow 3 | 0.3 | <u>48.3</u> | 60.1 | <u>63.8</u> | 58.0 |
| ✓ | ✓ | shallow 6 | 0.3 | 47.6 | 60.1 | <u>63.8</u> | 59.0 |
| ✓ | ✓ | deep 3 | 0.3 | 47.4 | 61.6 | 63.7 | <u>58.7</u> |
| ✓ | ✓ | deep 6 | 0.3 | 48.0 | 60.6 | 64.9 | 58.5 |
| ✓ | ✓ | deep 3 / deep 6 | 0.2 / 0.3 | 50.0 | 62.2 | 64.9 | 59.0 |

Table 8. **Ablation of Frequency Adapter with different activation layers.** The results demonstrate that the Earth-Adapter tends to be more beneficial when used in deeper network layers. The results in the gray shadow mean the best performance using deep 3 or 6 layers and 0.2 or 0.3 cutoff frequencies.

depth analysis of the hyperparameter effects.

Effect of Adapter dimension. The Earth-Adapter achieves optimal performance across varying dimensions on different benchmarks: P2V (DA) attains peak performance (67.3% mIoU at dim=64), P2V (DG) reaches its highest score (64.9% at dim=24), V2P (DA) achieves 62.2% mIoU at dim=32, while V2P (DG) attains its best performance at dim=64. A notable pattern emerges where domain generalization (DG) tasks consistently require larger-dimension adapters—V2P (DG) and R2U (DG) both peak at dim=64—whereas domain adaptation (DA) tasks achieve optimal results with smaller dimensions (V2P (DA) at dim=32 and R2U (DA) at dim=16). We attribute this phenomenon to DG tasks demanding greater parameter capacity to facilitate the foundation model’s extraction of more comprehensive semantic representations, thereby significantly boosting cross-domain generalization performance.

Effect of cutoff frequency. The cutoff frequency in the frequency domain serves as the boundary between high and low frequencies. Empirical evidence suggests that a relatively low cutoff value is generally preferable. In our experiments, we evaluated performance at cutoff frequencies of 0.2 and 0.3. Different benchmarks achieved optimal results at different frequencies: six benchmarks (P2V (DA), P2V (DG), V2P (DG), R2U (DA), R2U (DG), and U2R (DG)) attained peak performance at a cutoff ratio of 0.3, while V2P (DA) and U2R (DA) performed best at a ratio of 0.2.

Effect of Frequency Adapter layer. We also conducted experiments on the configuration of frequency-domain adapters across different layers. Our study primarily focused on the Dinov2-Large model, a 24-layer Vision Transformer architecture. We evaluated four distinct adapter configurations: {0,1,2}, {0,1,2,3,4,5}, {21,22,23}, and {18,19,20,21,22,23}. As shown in Table 6, different benchmarks achieved optimal performance with varying frequency-domain adapter configuration. For instance, P2V (DA) attained its peak performance of 67.7% mIoU with adapters in 0,1,2, while P2V (DG) achieved its best results with the {18,19,20,21,22,23} configuration. Similar to the adapter dimension findings, the frequency adapter lay-

ers demonstrate task-dependent optimization patterns. Notably, three DG tasks (P2V (DG), V2P (DG), and U2R (DG)) consistently performed best with adapters in the layers {18,19,20,21,22,23}, suggesting that domain generalization (DG) requires more adapter parameters to capture general semantic representations to improve cross-domain performance.

4.5. Discussion on Adapter Layer

Layer-wise comparison between Adapter and Earth-Adapter. We analyze the layer-wise behavior of Adapter and compare the performance of Adapter and Earth-Adapter under different layer configurations (Table 7). While prior work [68] suggests that deeper layers capture more semantically meaningful features, our Earth-Adapter demonstrates superior performance in both shallow-layer (first six) and deep-layer (last six) fine-tuning. For instance, in the U2R (DA) task, Earth-Adapter (shallow fine-tuning) outperforms the frozen model by 35.8% mIoU, while in R2U (DG), it surpasses the frozen baseline by 1.9% mIoU. Similar improvements are observed for deep-layer fine-tuning, achieving +38.2% mIoU (U2R (DA)) and +1.6% mIoU (U2R (DG)). Moreover, compared to Adapter, Earth-Adapter consistently shows better adaptation—+2.9% mIoU (U2R (DA), shallow) and +0.4% mIoU (R2U (DG), deep). These results highlight Earth-Adapter’s robustness and generalization capability across different layer-wise configurations.

Detailed analysis of parameter configuration of Frequency Adapter. We conduct a comprehensive analysis of the impact of frequency-domain layers on model performance, as shown in Table 8. In our default setting, the cutoff frequency of Earth-Adapter is set to 0.3. Our experiments reveal that these frequency layers play a crucial role in the overall performance of Earth-Adapter. Notably, integrating the Frequency Adapter results in a slight performance drop in two benchmarks: U2R (DA) (−1.6% mIoU) and R2U (DG) (−0.5% mIoU). However, with an efficient parameter search, Earth-Adapter still surpasses the Spatial Adapter. As shown in the table, Earth-Adapter achieves 50.0% mIoU in the U2R (DA) task, outperforming Spatial-Adapter by

1.4% mIoU. Similarly, it attains 59.0% mIoU in the R2U (DG) task, exceeding Spatial Adapter by 0.4% mIoU. A key observation is that Earth-Adapter exhibits sensitivity to frequency layer configurations and cutoff frequencies under certain benchmarks—an aspect we aim to refine in future work.

5. Conclusion

In this paper, we first highlight the performance drop when transferring existing PEFT methods to the RS cross-domain experiments. Detailedly, we analyze these problems through the research [12] and our artifacts-related findings, then raise that existing methods can not effectively handle the artifacts appearing in RS images. To tackle this, we introduce Earth-Adapter, our RS-specialized PEFT method. It is a simple-yet-effective and the first PEFT method for cross-domain RS semantic segmentation. In the experiment section, we first comprehensively evaluate Earth-Adapter’s performance and compare with other methods on widely-used benchmarks. Secondly, we analyze Earth-Adapter’s effectiveness with different backbones, as well as the trade-off between parameters, speed, and performance. Finally, we visualize the decoder’s predictions and expert outputs. Our results demonstrate Earth-Adapter’s power, efficiency, robustness, and explainability.

However, there is still space for improvement. For example, it’s still unclear on which backbone layers it should be applied, and how to further enhance the utilization of frequency features. In our subsequent work, we’ll pursue more potential optimization. The code will be public soon, and we hope Earth-Adapter will be helpful to this community.

References

- [1] Ahmed Agiza, Marina Neseem, and Sherief Reda. Mtlora: Low-rank adaptation approach for efficient multi-task learning. In *Proceedings of the IEEE/CVF Conference on Computer Vision and Pattern Recognition*, pages 16196–16205, 2024. 3
- [2] Qi Bi, Jingjun Yi, Hao Zheng, Haolan Zhan, Yawen Huang, Wei Ji, Yuexiang Li, and Yefeng Zheng. Learning frequency-adapted vision foundation model for domain generalized semantic segmentation. In *The Thirty-eighth Annual Conference on Neural Information Processing Systems*. 3
- [3] Rishi Bommasani, Drew A Hudson, Ehsan Adeli, Russ Altman, Simran Arora, Sydney von Arx, Michael S Bernstein, Jeannette Bohg, Antoine Bosselut, Emma Brunskill, et al. On the opportunities and risks of foundation models. *arXiv preprint arXiv:2108.07258*, 2021. 1, 3
- [4] Tom Brown, Benjamin Mann, Nick Ryder, Melanie Subbiah, Jared D Kaplan, Prafulla Dhariwal, Arvind Neelakantan, Pranav Shyam, Girish Sastry, Amanda Askell, et al. Language models are few-shot learners. *NeurIPS*, 33:1877–1901, 2020. 3
- [5] Keumgang Cha, Junghoon Seo, and Taekyung Lee. A billion-scale foundation model for remote sensing images. *arXiv preprint arXiv:2304.05215*, 2023. 1
- [6] Keyan Chen, Chenyang Liu, Hao Chen, Haotian Zhang, Wenyuan Li, Zhengxia Zou, and Zhenwei Shi. Rsprompter: Learning to prompt for remote sensing instance segmentation based on visual foundation model. *IEEE Transactions on Geoscience and Remote Sensing*, 2024. 3
- [7] Shoufa Chen, Chongjian Ge, Zhan Tong, Jiangliu Wang, Yibing Song, Jue Wang, and Ping Luo. Adaptformer: Adapting vision transformers for scalable visual recognition. *Advances in Neural Information Processing Systems*, 35:16664–16678, 2022. 5
- [8] Zhe Chen, Yuchen Duan, Wenhai Wang, Junjun He, Tong Lu, Jifeng Dai, and Yu Qiao. Vision transformer adapter for dense predictions. *arXiv preprint arXiv:2205.08534*, 2022. 1
- [9] Zhe Chen, Jiannan Wu, Wenhai Wang, Weijie Su, Guo Chen, Sen Xing, Muyan Zhong, Qinglong Zhang, Xizhou Zhu, Lewei Lu, et al. Internvl: Scaling up vision foundation models and aligning for generic visual-linguistic tasks. In *Proceedings of the IEEE/CVF conference on computer vision and pattern recognition*, pages 24185–24198, 2024. 3
- [10] Bowen Cheng, Ishan Misra, Alexander G Schwing, Alexander Kirillov, and Rohit Girdhar. Masked-attention mask transformer for universal image segmentation. In *Proceedings of the IEEE/CVF conference on computer vision and pattern recognition*, pages 1290–1299, 2022. 3, 5
- [11] MMSegmentation Contributors. MMSegmentation: Openmmlab semantic segmentation toolbox and benchmark. <https://github.com/open-mmlab/mms Segmentation>, 2020. 5
- [12] Timothée Darcet, Maxime Oquab, Julien Mairal, and Piotr Bojanowski. Vision transformers need registers. In *The Twelfth International Conference on Learning Representations*, 2024. 1, 10
- [13] Zhe Dong, Yanfeng Gu, and Tianzhu Liu. Upetu: A unified parameter-efficient fine-tuning framework for remote sensing foundation model. *IEEE Transactions on Geoscience and Remote Sensing*, 2024. 3
- [14] Alexey Dosovitskiy. An image is worth 16x16 words: Transformers for image recognition at scale. *arXiv preprint arXiv:2010.11929*, 2020. 1
- [15] Gamaleldin F Elsayed, Ian Goodfellow, and Jascha Sohl-Dickstein. Adversarial reprogramming of neural networks. *arXiv preprint arXiv:1806.11146*, 2018. 3
- [16] Kuiliang Gao, Anzhu Yu, Xiong You, Chunping Qiu, and Bing Liu. Prototype and context-enhanced learning for unsupervised domain adaptation semantic segmentation of remote sensing images. *IEEE Transactions on Geoscience and Remote Sensing*, 61:1–16, 2023. 3
- [17] Yunhe Gao, Xingjian Shi, Yi Zhu, Hao Wang, Zhiqiang Tang, Xiong Zhou, Mu Li, and Dimitris N Metaxas. Visual prompt tuning for test-time domain adaptation. *arXiv preprint arXiv:2210.04831*, 2022. 3
- [18] Chunjiang Ge, Rui Huang, Mixue Xie, Zihang Lai, Shiji Song, Shuang Li, and Gao Huang. Domain adaptation via

- prompt learning. *IEEE Transactions on Neural Networks and Learning Systems*, 2023. 3
- [19] Ziyang Gong, Fuhao Li, Yupeng Deng, Wenjun Shen, Xianzheng Ma, Zhenming Ji, and Nan Xia. Train one, generalize to all: Generalizable semantic segmentation from single-scene to all adverse scenes. In *Proceedings of the 31st ACM International Conference on Multimedia*, pages 2275–2284, 2023. 2
- [20] Ziyang Gong, Fuhao Li, Yupeng Deng, Deblina Bhattacharjee, Xianzheng Ma, Xiangwei Zhu, and Zhenming Ji. Coda: Instructive chain-of-domain adaptation with severity-aware visual prompt tuning. In *European Conference on Computer Vision*, pages 130–148. Springer, 2024. 1, 3
- [21] Ziyang Gong, Zhixiang Wei, Di Wang, Xianzheng Ma, Hongruixuan Chen, Yuru Jia, Yupeng Deng, Zhenming Ji, Xiangwei Zhu, Naoto Yokoya, et al. Crossearth: Geospatial vision foundation model for domain generalizable remote sensing semantic segmentation. *arXiv preprint arXiv:2410.22629*, 2024. 1, 2, 7
- [22] Albert Gu and Tri Dao. Mamba: Linear-time sequence modeling with selective state spaces. *arXiv preprint arXiv:2312.00752*, 2023. 1
- [23] Xin Guo, Jiangwei Lao, Bo Dang, Yingying Zhang, Lei Yu, Lixiang Ru, Liheng Zhong, Ziyuan Huang, Kang Wu, Dingxiang Hu, et al. Skysense: A multi-modal remote sensing foundation model towards universal interpretation for earth observation imagery. In *Proceedings of the IEEE/CVF Conference on Computer Vision and Pattern Recognition*, pages 27672–27683, 2024. 1, 3
- [24] Kaiming He, Xinlei Chen, Saining Xie, Yanghao Li, Piotr Dollár, and Ross Girshick. Masked autoencoders are scalable vision learners. In *Proceedings of the IEEE/CVF conference on computer vision and pattern recognition*, pages 16000–16009, 2022. 3
- [25] Jonathan Ho, Ajay Jain, and Pieter Abbeel. Denoising diffusion probabilistic models. *Advances in neural information processing systems*, 33:6840–6851, 2020. 1
- [26] Danfeng Hong, Bing Zhang, Xuyang Li, Yuxuan Li, Chenyu Li, Jing Yao, Naoto Yokoya, Hao Li, Pedram Ghamisi, Xiuping Jia, Antonio Plaza, Paolo Gamba, Jon Atli Benediktsson, and Jocelyn Chanussot. SpectralGPT: Spectral remote sensing foundation model. *IEEE Transactions on Pattern Analysis and Machine Intelligence*, pages 1–18, 2024. 3
- [27] Neil Houlsby, Andrei Giurgiu, Stanislaw Jastrzebski, Bruna Morrone, Quentin De Laroussilhe, Andrea Gesmundo, Mona Attariyan, and Sylvain Gelly. Parameter-efficient transfer learning for nlp. In *International Conference on Machine Learning*, pages 2790–2799. PMLR, 2019. 3
- [28] Neil Houlsby, Andrei Giurgiu, Stanislaw Jastrzebski, Bruna Morrone, Quentin De Laroussilhe, Andrea Gesmundo, Mona Attariyan, and Sylvain Gelly. Parameter-efficient transfer learning for nlp. In *International conference on machine learning*, pages 2790–2799. PMLR, 2019. 1, 3, 5
- [29] Lukas Hoyer, Dengxin Dai, and Luc Van Gool. Daformer: Improving network architectures and training strategies for domain-adaptive semantic segmentation. In *Proceedings of the IEEE/CVF conference on computer vision and pattern recognition*, pages 9924–9935, 2022. 2, 5
- [30] Lukas Hoyer, Dengxin Dai, and Luc Van Gool. Hrda: Context-aware high-resolution domain-adaptive semantic segmentation. In *European conference on computer vision*, pages 372–391. Springer, 2022. 2, 5
- [31] Edward J Hu, Yelong Shen, Phillip Wallis, Zeyuan Allen-Zhu, Yuanzhi Li, Shean Wang, Lu Wang, and Weizhu Chen. Lora: Low-rank adaptation of large language models. *arXiv preprint arXiv:2106.09685*, 2021. 1, 3, 5
- [32] Leiya Hu, Wanxuan Lu, Hongfeng Yu, Dongshuo Yin, Xian Sun, and Kun Fu. Tea: A training-efficient adapting framework for tuning foundation models in remote sensing. *IEEE Transactions on Geoscience and Remote Sensing*, 2024. 3
- [33] Reo Iizuka, Junshi Xia, and Naoto Yokoya. Frequency-based optimal style mix for domain generalization in semantic segmentation of remote sensing images. *IEEE Transactions on Geoscience and Remote Sensing*, 2023. 3
- [34] Sarmad F Ismael, Koray Kayabol, and Erchan Aptoula. Un-supervised domain adaptation for the semantic segmentation of remote sensing images via one-shot image-to-image translation. *IEEE Geoscience and Remote Sensing Letters*, 20: 1–5, 2023. 3
- [35] Johannes Jakubik, Sujit Roy, CE Phillips, Paolo Fraccaro, Denys Godwin, Bianca Zadrozny, Daniela Szwarcman, Carlos Gomes, Gabby Nyirjesy, Blair Edwards, et al. Foundation models for generalist geospatial artificial intelligence. *CoRR*, 2023. 1
- [36] Menglin Jia, Luming Tang, Bor-Chun Chen, Claire Cardie, Serge Belongie, Bharath Hariharan, and Ser-Nam Lim. Visual prompt tuning. In *European Conference on Computer Vision*, pages 709–727. Springer, 2022. 1, 3, 5
- [37] Shibo Jie and Zhi-Hong Deng. Fact: Factor-tuning for lightweight adaptation on vision transformer. In *Proceedings of the AAAI conference on artificial intelligence*, pages 1060–1068, 2023. 3
- [38] Alexander Kirillov, Eric Mintun, Nikhila Ravi, Hanzi Mao, Chloe Rolland, Laura Gustafson, Tete Xiao, Spencer Whitehead, Alexander C Berg, Wan-Yen Lo, et al. Segment anything. In *ICCV*, pages 4015–4026, 2023. 1, 3
- [39] Fuhao Li, Ziyang Gong, Yupeng Deng, Xianzheng Ma, Renrui Zhang, Zhenming Ji, Xiangwei Zhu, and Hong Zhang. Parsing all adverse scenes: Severity-aware semantic segmentation with mask-enhanced cross-domain consistency. In *Proceedings of the AAAI Conference on Artificial Intelligence*, pages 13483–13491, 2024. 2
- [40] Chenbin Liang, Weibin Li, Yunyun Dong, and Wenlin Fu. Single domain generalization method for remote sensing image segmentation via category consistency on domain randomization. *IEEE Transactions on Geoscience and Remote Sensing*, 2024. 3
- [41] Fan Liu, Delong Chen, Zhangqingyun Guan, Xiaocong Zhou, Jiale Zhu, Qiaolin Ye, Liyong Fu, and Jun Zhou. Remoteclip: A vision language foundation model for remote sensing. *IEEE Transactions on Geoscience and Remote Sensing*, 2024. 1, 3
- [42] Haotian Liu, Chunyuan Li, Qingyang Wu, and Yong Jae Lee. Visual instruction tuning. *Advances in neural information processing systems*, 36:34892–34916, 2023. 3

- [43] Ze Liu, Yutong Lin, Yue Cao, Han Hu, Yixuan Wei, Zheng Zhang, Stephen Lin, and Baining Guo. Swin transformer: Hierarchical vision transformer using shifted windows. In *Proceedings of the IEEE/CVF international conference on computer vision*, pages 10012–10022, 2021. 1, 3
- [44] Jonathan Long, Evan Shelhamer, and Trevor Darrell. Fully convolutional networks for semantic segmentation. In *Proceedings of the IEEE conference on computer vision and pattern recognition*, pages 3431–3440, 2015. 2
- [45] Ilya Loshchilov and Frank Hutter. Decoupled weight decay regularization. In *International Conference on Learning Representations*, 2019. 5
- [46] Gen Luo, Xue Yang, Wenhan Dou, Zhaokai Wang, Jifeng Dai, Yu Qiao, and Xizhou Zhu. Mono-internvl: Pushing the boundaries of monolithic multimodal large language models with endogenous visual pre-training. *arXiv preprint arXiv:2410.08202*, 2024. 3
- [47] ITC Markus Gerke. Use of the stair vision library within the isprs 2d semantic labeling benchmark (vaihingen). *Use of the stair vision library within the isprs 2d semantic labeling benchmark (vaihingen)*, 2014. 4
- [48] Matias Mendieta, Boran Han, Xingjian Shi, Yi Zhu, Chen Chen, and Mu Li Gfm. Building geospatial foundation models via continual pretraining. *arXiv preprint arXiv:2302.04476*, 6(7), 2023. 1
- [49] Maxime Oquab, Timothée Darcet, Théo Moutakanni, Huy Vo, Marc Szafraniec, Vasil Khalidov, Pierre Fernandez, Daniel Haziza, Francisco Massa, Alaaeldin El-Nouby, et al. Dinov2: Learning robust visual features without supervision. *arXiv preprint arXiv:2304.07193*, 2023. 3, 5
- [50] Xinyang Pu and Feng Xu. Low-rank adaption on transformer-based oriented object detector for satellite on-board processing of remote sensing images. *IEEE Transactions on Geoscience and Remote Sensing*, 2025. 3
- [51] Alec Radford, Jong Wook Kim, Chris Hallacy, Aditya Ramesh, Gabriel Goh, Sandhini Agarwal, Girish Sastry, Amanda Askell, Pamela Mishkin, Jack Clark, et al. Learning transferable visual models from natural language supervision. In *International conference on machine learning*, pages 8748–8763. PmLR, 2021. 1, 3, 5
- [52] Robin Rombach, Andreas Blattmann, Dominik Lorenz, Patrick Esser, and Björn Ommer. High-resolution image synthesis with latent diffusion models. In *Proceedings of the IEEE/CVF conference on computer vision and pattern recognition*, pages 10684–10695, 2022. 1
- [53] Zhang Rui and Li Jintao. A survey on algorithm research of scene parsing based on deep learning. *Journal of Computer Research and Development*, 57(4):859–875, 2020. 3
- [54] Evan Shelhamer, Jonathan Long, and Trevor Darrell. Fully convolutional networks for semantic segmentation. *IEEE transactions on pattern analysis and machine intelligence*, 39(4):640–651, 2016. 2
- [55] Subhashree Subudhi, Ram Narayan Patro, Pradyut Kumar Biswal, and Fabio Dell’Acqua. A survey on superpixel segmentation as a preprocessing step in hyperspectral image analysis. *IEEE Journal of Selected Topics in Applied Earth Observations and Remote Sensing*, 14:5015–5035, 2021. 3
- [56] Jiachen Sun, Mark Ibrahim, Melissa Hall, Ivan Evtimov, Z Morley Mao, Cristian Canton Ferrer, and Caner Hazirbas. Vpa: Fully test-time visual prompt adaptation. In *Proceedings of the 31st ACM International Conference on Multimedia*, pages 5796–5806, 2023. 3
- [57] Xin-Yi Tong, Gui-Song Xia, Qikai Lu, Huanfeng Shen, Shengyang Li, Shucheng You, and Liangpei Zhang. Land-cover classification with high-resolution remote sensing images using transferable deep models. *Remote Sensing of Environment*, 237:111322, 2020. 3
- [58] Wilhelm Tranehden, Viktor Olsson, Juliano Pinto, and Lennart Svensson. Dacs: Domain adaptation via cross-domain mixed sampling. In *Proceedings of the IEEE/CVF winter conference on applications of computer vision*, pages 1379–1389, 2021. 4
- [59] Di Wang, Jing Zhang, Bo Du, Minqiang Xu, Lin Liu, Dacheng Tao, and Liangpei Zhang. SAMRS: Scaling-up remote sensing segmentation dataset with segment anything model. In *NeurIPS*, pages 8815–8827, 2023. 3
- [60] Di Wang, Qiming Zhang, Yufei Xu, Jing Zhang, Bo Du, Dacheng Tao, and Liangpei Zhang. Advancing plain vision transformer toward remote sensing foundation model. *IEEE Transactions on Geoscience and Remote Sensing*, 61:1–15, 2023.
- [61] Di Wang, Meiqi Hu, Yao Jin, Yuchun Miao, Jiaqi Yang, Yichu Xu, Xiaolei Qin, Jiaqi Ma, Lingyu Sun, Chenxing Li, Chuan Fu, Hongruixuan Chen, Chengxi Han, Naoto Yokoya, Jing Zhang, Minqiang Xu, Lin Liu, Lefei Zhang, Chen Wu, Bo Du, Dacheng Tao, and Liangpei Zhang. Hypersigma: Hyperspectral intelligence comprehension foundation model. *arXiv preprint arXiv:2406.11519*, 2024. 3
- [62] Di Wang, Jing Zhang, Minqiang Xu, Lin Liu, Dongsheng Wang, Erzong Gao, Chengxi Han, Haonan Guo, Bo Du, Dacheng Tao, et al. Mtp: Advancing remote sensing foundation model via multi-task pretraining. *IEEE Journal of Selected Topics in Applied Earth Observations and Remote Sensing*, 2024. 1
- [63] Junjie Wang, Zhuo Zheng, Ailong Ma, Xiaoyan Lu, and Yanfei Zhong. Loveda: A remote sensing land-cover dataset for domain adaptive semantic segmentation. *arXiv preprint arXiv:2110.08733*, 2021. 4
- [64] Zhixiang Wei, Lin Chen, Yi Jin, Xiaoxiao Ma, Tianle Liu, Pengyang Ling, Ben Wang, Huaian Chen, and Jinjin Zheng. Stronger fewer & superior: Harnessing vision foundation models for domain generalized semantic segmentation. In *Proceedings of the IEEE/CVF Conference on Computer Vision and Pattern Recognition (CVPR)*, pages 28619–28630, 2024. 2, 3, 5
- [65] Enze Xie, Wenhai Wang, Zhiding Yu, Anima Anandkumar, Jose M Alvarez, and Ping Luo. Segformer: Simple and efficient design for semantic segmentation with transformers. *Advances in neural information processing systems*, 34: 12077–12090, 2021. 5
- [66] Dongshuo Yin, Yiran Yang, Zhechao Wang, Hongfeng Yu, Kaiwen Wei, and Xian Sun. 1% vs 100%: Parameter-efficient low rank adapter for dense predictions. In *Proceedings of the IEEE/CVF Conference on Computer Vision and Pattern Recognition*, pages 20116–20126, 2023. 3

- [67] Zhiping Yu, Chenyang Liu, Liqin Liu, Zhenwei Shi, and Zhengxia Zou. Metaearth: A generative foundation model for global-scale remote sensing image generation. *arXiv preprint arXiv:2405.13570*, 2024. [1](#), [3](#)
- [68] Linfeng Zhang, Jiebo Song, Anni Gao, Jingwei Chen, Chenglong Bao, and Kaisheng Ma. Be your own teacher: Improve the performance of convolutional neural networks via self distillation. In *Proceedings of the IEEE/CVF international conference on computer vision*, pages 3713–3722, 2019. [9](#)
- [69] Jingru Zhu, Ya Guo, Geng Sun, Libo Yang, Min Deng, and Jie Chen. Unsupervised domain adaptation semantic segmentation of high-resolution remote sensing imagery with invariant domain-level prototype memory. *IEEE Transactions on Geoscience and Remote Sensing*, 61:1–18, 2023. [3](#)